High Thermoelectric Power Conversion Efficiency of an Earth-Abundant Janus Silicon Oxy-Sulfide Monolayer: A First-Principles Study

Zakariae Darhi[a]*, Mounaim bencheikh[a], Ravindra Pandey[b], Larbi El Farh[a]

[a]*Mohammed First University, Faculty of Sciences, Department of Physics, Oujda 60000, Morocco*
[b]*Michigan Technological University, Department of Physics, 1400 Townsend Drive, Houghton, MI 49931, USA*

(January 2026)

*Corresponding Author: zakariae.darhi@ump.ac.ma

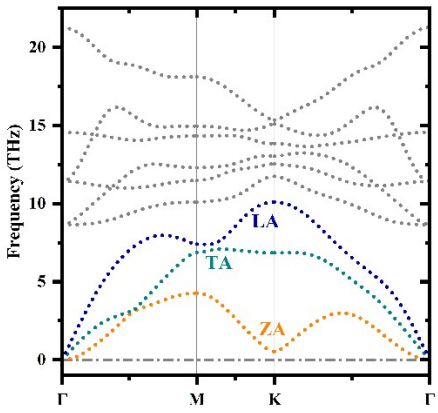

Fig. S1 Corrected harmonic phonon spectra of the Janus SiOS monolayer calculated using hiphive with a 6×6×1 supercell.

Analytical expressions for the angular dependence of the in-plane Young's modulus and Poisson's ratio.

$$Y(\theta) = \frac{C_{11}C_{22} - C_{12}^2}{C_{22}\sin\theta^4 + C_{11}\cos\theta^4\theta + \left(\frac{C_{11}C_{22} - C_{12}^2}{C_{66}} - 2C_{12}\right)\sin\theta^2\cos\theta^2} \#(1)$$

$$\nu(\theta) = \frac{C_{12}(\cos\theta^4 + \sin\theta^4) - \left(C_{11} + C_{22} - \frac{C_{11}C_{22} - C_{12}^2}{C_{66}}\right)\sin\theta^2\theta\cos\theta^2}{C_{22}\sin\theta^4 + C_{11}\cos\theta^4 + \left(\frac{C_{11}C_{22} - C_{12}^2}{C_{66}} - 2C_{12}\right)\sin\theta^2\theta\cos\theta^2} \#(2)$$

Where $C_{66} = \frac{C_{11} - C_{12}}{2}$ and θ is the in-plane angle.

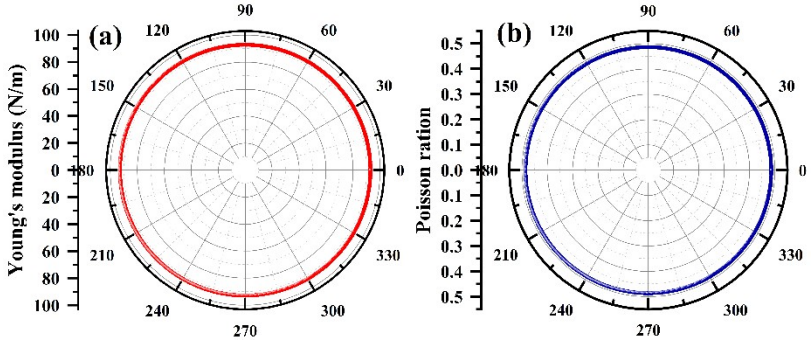

Fig. S2 Angular dependence of the (a) Young's modulus (b) shear modulus of the Janus SiOS monolayer.

Table S1 Calculated elastic constants (C_{ij}), Young's modulus (Y), and Poisson ration (ν).

$C_{11}\ (N/m)$	$C_{12}\ (N/m)$	$C_{66}\ (N/m)$	$Y\ (N/m)$	ν
121.39	58.99	31.20	92.72	0.486

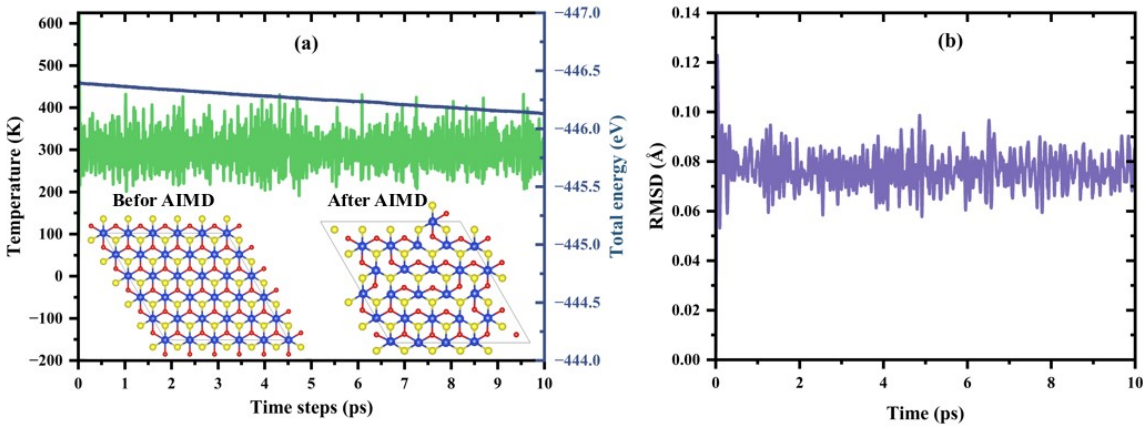

Fig. S3 (a) AIMD simulations of the total energy (in bule) and temperature (in green) and (b) root-mean-square displacement (RMSD) versus time step at 300 K.

Convergence Details for Lattice thermal conductivity

To ensure convergence, the thermal conductivity calculations were validated using the method of Qin and Hu [1], which analyzes interatomic interactions. Thus, we chose the cutoff distances from the RMS values of the second-order IFC elements

$$RMS\left(\phi_{ij}\right) = \left[\frac{1}{9}\sum_{\alpha,\beta}\left(\phi_{ij}^{\alpha\beta}\right)^2\right]^{\frac{1}{2}} \#(1)$$

Where ϕ_{ij} is the second-order IFCs between atom i in direction α and j in direction β. As shown in Fig. S2 (a), the strength of these interactions decreases with increasing interatomic distance. A cutoff distance of 5.29 Å, corresponding to the interaction with the 8th nearest neighbor, was selected to achieve an optimal balance between computational efficiency and the accurate representation of significant interatomic interactions.

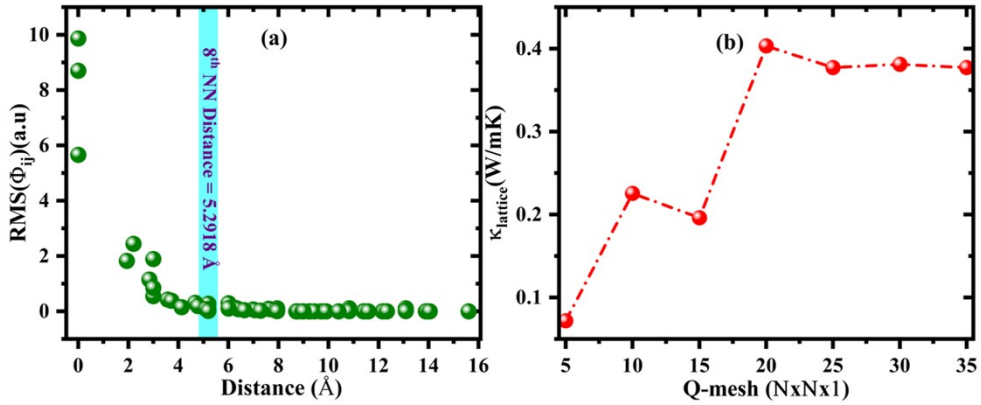

Fig. S4 (a) Calculated RMS vs. cutoff distance and (b) the convergence test of lattice thermal conductivity with the variation in the Q-grid.

Detailed input parameters used in AMSET and ShengBTE

- **Macroscopic static dielectric tensor-ionic contribution**

3.015759	0.000000	0.000000
0.000000	3.015759	-0.000000
0.000000	-0.000000	0.018692

- **Macroscopic static dielectric tensor- Electronic (high-frequency) contribution**

2.413474	0.000000	0.000000
0.000000	2.413474	-0.000000
0.000000	-0.000000	1.229162

- **Born effective charges (in |e|)**

	ion 1		
1	4.13378	0.00000	0.00000
2	0.00000	4.13378	0.00000
3	0.00000	-0.00000	0.64899
	ion 2		
1	-2.30849	-0.00000	-0.00000
2	-0.00000	-2.30849	-0.00000
3	-0.00000	0.00000	-0.45830
	ion 3		
1	-1.82528	-0.00000	-0.00000
2	-0.00000	-1.82528	-0.00000
3	-0.00000	0.00000	-0.19069

- **The deformation potential constant** (E_d)

The band deformation potential quantifies the variation in the CBM (Conduction Band Minimum) or VBM (Valence Band Maximum) energies of the Janus SiOS monolayer under uniaxial strains ranging from -2% to +2% in increments of 0.5%.

$$E_d = \frac{dE_{edge}}{d\varepsilon} \#(1)$$

Table S2 Calculated deformation potential $(E_d(eV))$, high-frequency dielectric constant (ε_∞), static dielectric constant $(\varepsilon_0 = \varepsilon_\infty + \varepsilon_{ionic})$, polar phonon frequency $(\hbar\omega_{pop}(THz))$

Carriers	$E_d(eV)$	ε_∞	ε_0	$\hbar\omega_{pop}(THz)$
electrons	-9.06	2.41	5.42	10.32
holes	-13.52	2.41	5.42	10.32

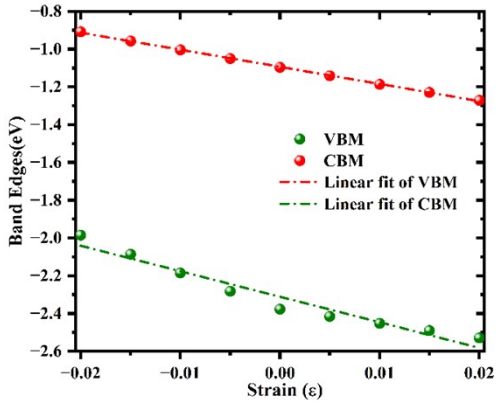

Fig. S5 Calculated band edge positions and their linear fitting for the Janus SiOS monolayer.

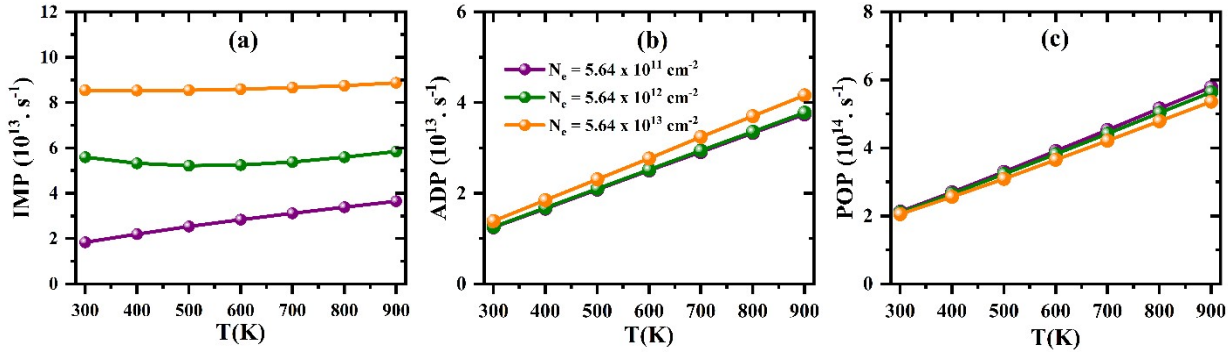

Fig. S6 Calculated (a) ionized impurity (IMP), (b) acoustic deformation potential (ADP), and (c) polar optical phonon (POP) scattering as functions of charge carrier concentration for the n-type Janus SiOS monolayer at different temperatures.

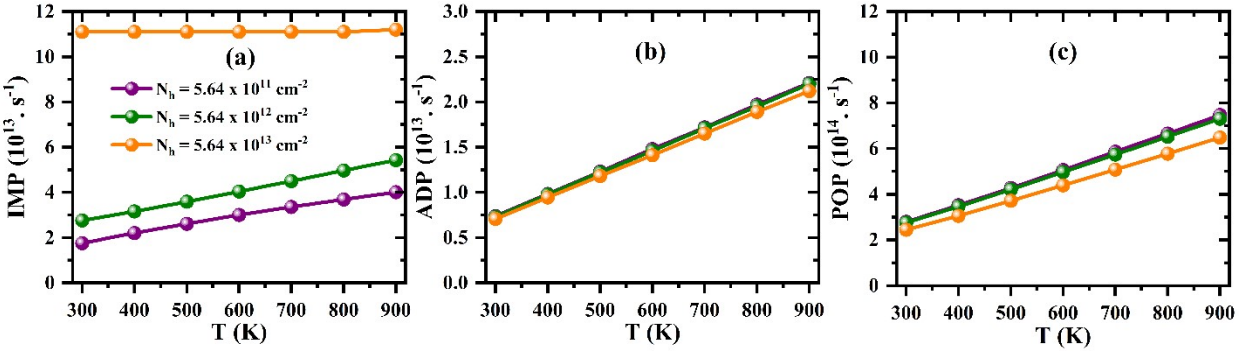

Fig. S7 Calculated (a) ionized impurity (IMP), (b) acoustic deformation potential (ADP), and (c) polar optical phonon (POP) scattering as functions of charge carrier concentration for the p-type Janus SiOS monolayer at different temperatures.

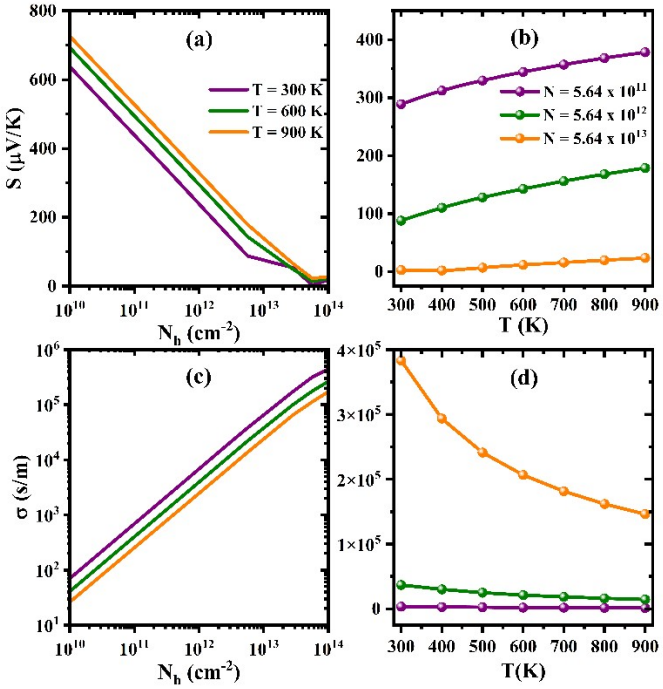

Fig. S8 Calculated absolute Seebeck coefficient (|S|) and electrical conductivity (σ) versus (a, c) carrier concentration (N_h) and (b, d) temperature (T) for the p-type Janus SiOS monolayer.

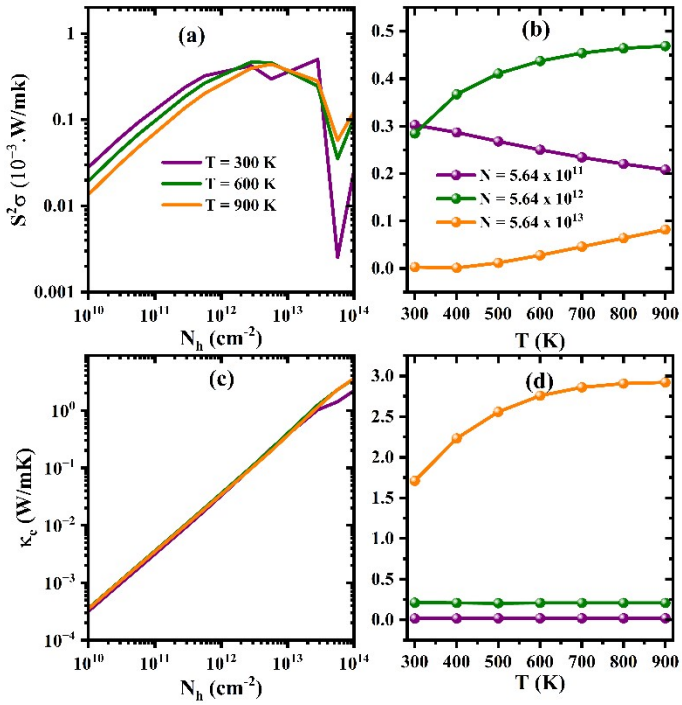

Fig. S9 Calculated power factor ($S^2\sigma$) and electronic thermal conductivity ( ) (a, c) versus carrier concentration ( ) (b, d) and temperature (T) for the p-type Janus SiOS monolayer.

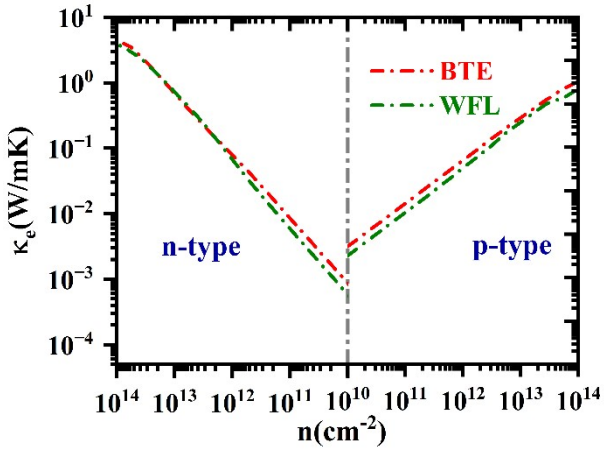

Fig. S10 Calculated electronic thermal conductivity and figure of merit by employing the Boltzmann transport equation (BTE) and Wiedemann-Franz law (WFL) at 300 K for n and p-type for The Janus SiOS monolayer.

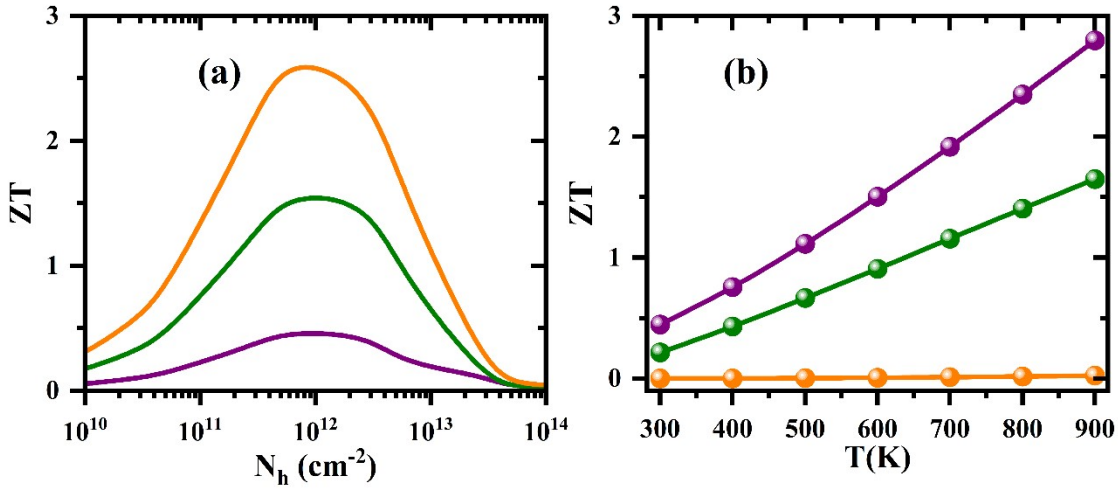

Fig. S11 Calculated figure of merit (ZT) versus (a) carrier concentration (^{N_h}) and (b) temperature (T) for the p-type Janus SiOS monolayer

[1] G. Qin, M. Hu, npj Computational Materials, 4 (2018) 3.